THE JOURNAL OF Pathology
A Journal of The Pathological Society
Understanding Disease

Functional molecules in mesothelial to mesenchymal transition revealed by transcriptome analyses

Journal:	*The Journal of Pathology*
Manuscript ID	17-692.R1
Wiley - Manuscript type:	Original Research Article
Date Submitted by the Author:	n/a
Complete List of Authors:	Namvar, Sara; University of Manchester, Division of Cell Matrix Biology and Regenerative Medicine, School of Biological Sciences, Faculty of Biology Medicine and Health; University of Manchester, Faculty of Biology Medicine and Health Woolf, Adrian; University of Manchester, Division of Cell Matrix Biology and Regenerative Medicine, School of Biological Sciences, Faculty of Biology Medicine and Health; Manchester Academic Health Science Centre, University of Manchester; university of manchester, Division of Cell Matrix Biology and Regenerative Medicine, School of Biological Sciences, FBMH Zeef, Leo; University of Manchester, Faculty of Biology Medicine and Health Wilm, Thomas; University of Liverpool Institute of Translational Medicine, Translational Medicine Wilm, Bettina; University of Liverpool Institute of Translational Medicine, Translational Medicine Herrick, Sarah; University of Manchester , Division of Cell Matrix Biology and Regenerative Medicine, School of Biological Sciences, Faculty of Biology Medicine and Health
Tissue:	
Pathology:	
Technique:	

Functional molecules in mesothelial-to-mesenchymal transition revealed by transcriptome analyses

Sara Namvar[1,2], Adrian S. Woolf[1,2,3], Leo A.H. Zeef[1,2], Thomas Wilm[4], Bettina Wilm[4] and Sarah E. Herrick[1,2].

[1]Division of Cell Matrix Biology and Regenerative Medicine, School of Biological Sciences, Faculty of Biology Medicine and Health, University of Manchester, UK.

[2]Manchester Academic Health Science Centre, Manchester, UK.

[3]Royal Manchester Children's Hospital, Manchester University NHS Foundation Trust, Manchester, UK.

[4]Institute of Translational Medicine, University of Liverpool, UK.

Corresponding author

Sarah E Herrick, 3.106 Stopford Building, Faculty of Biology, Medicine and Health, The University of Manchester, Manchester M13 9PT. UK. Phone +44 (0)161 275 1528, Fax +44 (0)161 275 1813. E-mail sarah.herrick@manchester.ac.uk

Running title: Mesothelial molecular signatures

Conflict of interest statement

All authors declare no conflicts of interest.

RNA-seq data is available on ArrayExpress E-MTAB-5998.

Abstract

Peritoneal fibrosis is a common complication of abdominal and pelvic surgery, and it can also be triggered by peritoneal dialysis resulting in treatment failure. In these settings, fibrosis is driven by activated myofibroblasts that are considered to be partly derived by mesothelial-to-mesenchymal transition (MMT). We hypothesised that if the molecular signature of MMT could be better defined, these insights could then be exploited to functionally block this pathological cellular transition. Using an antibody to HBME1, a protein present on mesothelial cell microvilli, and streptavidin nanobead technology, rat peritoneal mesothelial cells were purified and cultured. After exposing sorted cells to a well-known mediator of MMT, transforming growth factor β1 (TGFβ1), RNA sequencing was undertaken to define the transcriptomes of mesothelial cells before and during early phase MMT. MMT was associated with dysregulation of transcripts encoding molecules involved in insulin-like growth factor (IGF) and bone morphogenetic factor (BMP) signalling. The application of either recombinant BMP4 or IGF binding protein 4 (IGFBP4) ameliorated TGFβ1-induced MMT in culture as evidenced by the retention of epithelial morphological and molecular phenotypes, and reduced migration. Furthermore, compared with control tissue, peritoneal tissue from peritoneal dialysis patients showed less prominent immunostaining for IGFBP4 and BMP4 on the peritoneal surface. In a mouse model of TGFβ1-induced peritoneal thickening, BMP4 immunostaining on the peritoneal surface was attenuated compared with healthy controls. Finally, genetic lineage tracing of mesothelial cells was used in mice with peritoneal injury. In this model, administration of BMP4 ameliorated the injury-induced shape change and migration

of mesothelial cells. Our findings demonstrate a distinctive MMT signature and highlight the therapeutic potential for BMP4, and possibly IGFBP4, to reduce MMT.

Key words bone morphogenetic protein, insulin-like growth factor, peritoneum, mesothelium

Introduction

Epithelia form sheets and tubules conferring physical integrity and physiological function. Epithelial-to-mesenchymal transition (EMT) occurs in normal development during gastrulation and neural crest migration. EMT is characterised by disrupted cell-cell adhesion and apical-basolateral polarity, cytoskeletal reorganisation, detachment from basement membranes, and generation of motile mesenchymal cells. The reverse process, mesenchymal-to-epithelial transition (MET), occurs during somitogenesis and nephrogenesis [1,2]. Mesothelial cells (MCs) are epithelial-like cells lining the coelomic cavities and the organs they contain. MCs have junctional complexes and apical-basolateral polarity, and adhere to a basement membrane. MCs secrete glycosaminoglycans and surfactant, permitting frictionless gliding of organs, and act as a barrier expressing inflammation-modulating cytokines. MCs *in vivo* not only express cytokeratins, characteristic of epithelia, but also vimentin, more typical of mesenchyme [3]. In normal development, some MCs undergo mesothelial-to-mesenchymal transition (MMT) to form vascular smooth muscle [4,5]. In development and cancer, snail, twist and slug transcription factors drive EMT [6,7]. MCs are not typical epithelia, so MMT and EMT biology may not be identical.

Fibrosis is an aberrant response to injury and therapies to slow or reverse fibrosis are urgently needed. Alpha-smooth muscle actin (αSMA) expressing myofibroblasts drive fibrosis, and EMT is proposed to generate some of these cells [1,8]. In response to injury, MCs can undergo MMT [9-13]. For example, after injection of labelled MCs into the peritoneal cavity, they appear in the regenerating mesothelial

layer and in the sub-mesothelial layer [14]. Peritoneal fibrosis can be triggered by peritoneal dialysis, causing treatment failure, as well as surgery, causing adhesions. So, targeting MMT may prevent scarring. Mesothelial damage by peritoneal dialysis or surgery initiates production of pro-fibrotic mediators, notably transforming growth factor β1 (TGFβ1) [3]. We hypothesised that if the molecular signature of TGFβ1-induced MMT could be defined, these insights could be exploited to ameliorate MMT.

Materials and Methods

Animal experiments were undertaken according to ARRIVE guidelines and were approved by Review Boards of the Universities of Manchester and Liverpool, and by the Home Office.

Isolation, purification and culture of rat MCs

Omental tissue was dissected from adult 9-12 week old female Wistar rats weighing 220-250g (Charles River, Cambridgeshire, UK). Tissue was dissociated in 0.25% trypsin-EDTA (Sigma-Aldrich, Dorset, UK) for 20 min at 37°C. Cells were incubated with HBME1 antibody (Dako, Cambridge, UK) 1:50 for 30 min in 3% BSA in PBS. Cells were washed and incubated for 30 min with biotinylated secondary antibody (1:100; Vector Laboratories, Peterborough, UK). Following further washes, $1.5x10^6$ cells were incubated with streptavidin-coated magnetic nanobeads (Biolegend, London, UK) for 15 min, then placed in a MojoSort™ magnet (Biolegend) for 5 min. Uncaptured cells were decanted and the remainder resuspended in culture media comprising DMEM, high glucose supplemented with 15% FCS, 4 mM L-glutamine (Sigma-Aldrich), 1% v/v penicillin/streptomycin and 0.4 µg/ml hydrocortisone (Sigma-Aldrich). In other experiments, cells from trypsinized omentum underwent FACS sorting, as described [15]. Cells were processed as for magnetic bead sorting but HBME1 antibody was detected with IgM Alexa488 (1:1000; Thermo Fisher Scientific, Runcorn, UK). Cells were seeded at $5x10^4$ per cm^2 in multi-well plates. After comparing the two methods, subsequent experiments were performed using Mojo-purification. After 48-72 h of culture following enrichment, cells were washed with HBSS and media changed every other day for up to 10-11 days. Cells were then

placed in low serum (5% FCS) media. Cells were exposed to 1 ng/ml TGFβ1 for 48h (R&D Systems, Abington, UK) and/or 50 ng/ml bone morphogenetic protein (BMP4; Biolegend) and/or 50 ng/ml insulin-like growth factor binding protein 4 (IGFBP4; Biolegend).

RNA sequencing (RNA-seq) and quantitative polymerase chain reaction (QPCR)

These are detailed in the *Supplementary Information*. For RNA-seq, differentially expressed transcripts were defined as those showing at least a 0.36 log2-fold increase or decrease *versus* controls, and a statistical significance of $P<0.05$ corrected for multiple comparisons. The transcriptome data set is deposited in the ArrayExpress repository (E-MTAB-5998).

Immunostaining rat tissues, cell migration assay and ELISA

Details are found in *Supplementary Information*

TGFβ1-induced peritoneal fibrosis and peritoneal MC lineage tracing in mice.

Two models of peritoneal injury were studied. The first analysed tissues collected from wild-type C57 BL6J mice that had received intraperitoneal adenovirus expressing TGFβ1. We previously described that this led to submesothelial fibrosis *in vivo* [16]. In a second model, we combined surgical abrasion of the peritoneum [17] with a MC lineage tracing strategy, similar to that described by Lua *et al*, [18] but using *LacZ* rather than *GFP*. Detailed protocols are found in *Supplementary Information*.

Human tissue analyses

After informed patient consent and ethical approval (REC 06/Q1407/94), peritoneum was collected from individuals undergoing hernia repair (n=4) and from end-stage kidney disease patients who had undergone peritoneal dialysis (n=4). Tissues were fixed in 4% PFA for 24 h, and processed into paraffin blocks. Seven μm sections were permeabilised with 0.2% Triton in PBS, then incubated with primary antibodies to HBME1 (1:50; Dako), IGFBP4 (1:700; Abcam) or BMP4 (1:100; Abcam) overnight at 4˚C. Sections were incubated with Rabbit IgG Specific HRP/DAB (ABC) detection kit (Abcam). Images were obtained using a light microscope (Olympus) and image Pro Plus software (Media Cybernetics, Cambridge UK).

Statistics

Analysis for RNA sequencing data is outlined above. All other data sets were normally distributed, so presented as mean±SEM. Student's t-tests or ANOVA with Tukey post hoc tests were used to compare groups. Analyses were performed with GraphPad Prism 6 (GraphPad Software).

Results

MC enrichment

In rat omentum sections, HBME1 was immunodetected in MCs (Figure1A) but adipose and connective tissue were negative. Primary cultures of omental cells that had been selected after binding to the HBME1 antibody either by FACS or magnetic bead sorting (Mojo) showed an enhanced cobblestone appearance *versus* unsorted cells (Figure 1B). Compared with unsorted cells, FACS or magnetic bead sorting each resulted in significant enrichment of cells expressing HBME1 (Figure 1B and C) or Wt1 (Figure 1B and D), a MC transcription factor [4,5]. Unsorted cells showed a mean value for the level of HBME1 immunostaining of approximately 27,000 pixels/nucleus that rose significantly after either HBME1 FACS to 162,000 (P=0.022) or magnetic bead sorting to 192,000 (P=0.005). Wt1 was immunodetected in approximately half of all nuclei of unsorted cells, rising to 90% after HBME1 FACS sorting (P=0.022) and to 92% after HBME1 magnetic bead sorting (P=0.017).

Induction of MMT in cell culture

Mojo-sorted MCs were exposed to TGFβ1, a driver of both MMT and also peritoneal fibrosis [19,20]. After 48 h, untreated MCs maintained their cobblestone morphology (Figure 1E), whereas parallel cultures exposed to 1 ng/ml TGFβ1 progressively lost their epithelioid appearance and acquired an irregular elongated morphology (Figure 1E). Primary cultures of sorted cells displayed positive immunostaining for ZO1, a tight junction protein, and vimentin, an intermediate filament protein (Figure 1F) as expressed by MCs *in vivo* [21,22]. Immunostaining for E-cadherin was barely detectable, whereas MCF7 breast epithelial cells showed prominent cell-cell junction

immunostaining (Supplementary Figure S1). Using immunohistochemistry, the mesothelial layer of rat omentum *in vivo* was negative for E-cadherin, while nearby pancreatic ductal cells were positive (Supplementary Figure S1). In TGFβ1-exposured Mojo-sorted MCs: ZO1 became less prominent at cell-cell junctions, instead appearing in a cytoplasmic pattern; vimentin appeared more prominent; and αSMA, a smooth muscle contractile protein, appeared upregulated *versus* untreated cells (Figure 1F). Therefore, this protocol induced certain phenotypic changes considered typical of MMT [23,24].

Gene expression in purified MCs

To define the transcriptome of purified MCs we undertook RNA-seq. The complete dataset are is available in the ArrayExpress repository (E-MTAB-5998). In MCs exposed to 1 ng/ml TGFβ1 for 48 h, 834 species of transcripts increased, and 487 decreased, *versus* cells cultured without exogenous TGFβ1. Unsupervised hierarchical clustering clearly distinguished between the two groups (Figure 2A). The volcano plot in Figure 2B is annotated for changed *'epithelial signature'* transcripts, with Table 1 showing a list of changed transcripts in this class. Among downregulated transcripts were: *Cng*, encoding the tight junction protein cingulin; *Cldn2* and *Cldn15*, encoding tight junction claudins; *Col4a3* and *Col4a4*, encoding epithelial basement membrane collagens; *Itga3*, *Itga6*, *Itgb3* and *Itgb4*, encoding integrins; *Krt13*, *Krt18*, *Krt19* and *Krt23*, encoding keratin intermediate filaments; *Lamb2* and *Lamb3*, encoding laminin B2 and 3; *Podxl*, encoding silaomucin podocalyxin-like protein 1; *Ppl*, encoding the desmosomal protein periplakin; and *Upk3b*, encoding uroplakin 3B, a plasma membrane protein characteristic of mesothelia *in vivo* [25]. Control cells expressed high levels of transcripts for *Wt1*, and

for *Msln* encoding the glycosylphosphatidylinositol-anchored cell-surface protein mesothelin [26], but only low levels of *Cdh1*, encoding the cell-cell adhesion protein, E-cadherin. Moreover, levels of these three transcripts did not significantly change upon TGFβ1 exposure. Notably, *Sfn* levels rose after exposure to TGFβ1: the transcript encodes stratifin that has been linked to epithelial differentiation [27]. QPCR was undertaken (Figure 2C) for a subset of transcripts (*Cdh1, Cng*, *Col4a3*, *Col4a4*, *Pdxl*, *Snai1, Tjp1*, *Upk3b*, and *Vim*), with generally similar conclusions to the RNA-seq findings, although the fall in *Tjp1* was not significant. Notably, *Cdh1* transcripts were detectable but very low in the RNA-seq and unchanged by TGFβ1 (Table 1). E-cadherin, the encoded protein, was not detected *in vivo* was barely detected in cultured MCs (Supplementary Figure S1).

A selection of 'm*esenchymal/extracellular matrix signature'* transcripts is shown in Table 2. TGFβ1 exposure led to an increase in transcripts for *Acta2*, encoding αSMA, and *Vim*, encoding vimentin. These fold increases, however, were exceeded by those for the following transcripts: *Ncam1* and *Vcam1*, encoding neural and vascular cell adhesion molecules respectively; and *Tnc* and *Tnn*, encoding tenascin C and tenascin N respectively, both extracellular matrix glycoproteins. Table 3 lists transcripts previously implicated in classical EMT. A shown in Table 3, the following transcripts were upregulated: *Tgfb1*, *2* and *3*; *Snai1* and *Snai2*, encoding snail zinc finger proteins 1 and 2. We found that levels of *Twist 1* and *2*, encoding transcription factors considered key effectors of classical EMT [1,28], were not significantly altered by TGFβ1 (as shown in Table 3).

MMT is associated with altered transcripts of BMP and IGF pathway molecules

RNA-seq (Figure 3A and Table 4) revealed that control MCs expressed high levels of *Bmp4* transcripts but low levels of *Bmp7*. *Bmp4* was markedly downregulated upon exposure to TGFβ1, whereas levels for *Grem2*, that encodes the BMP antagonist, gremlin 2 [29], increased markedly as did *Bmp1*, encoding an atypical BMP family member that is a secreted metalloprotease implicated in cartilage formation [30]. TGFβ1 exposure led to increases in *Igf1* and *Igf2*, respectively encoding insulin-like growth factors I and II. *Igfbp2*, *Igfbp4*, *Igfbp5* and *Igfbp6* decreased. These encode IGFBPs that alter the interaction of IGFs with their cell surface receptors, usually decreasing IGF signalling [31]. We also detected marked increased levels of *Pappa* that encodes pregnancy-associated plasma protein A, a secreted metalloproteinase that cleaves IGFBPs, rendering them inactive [32]. Using QPCR, *Bmp4* and *Igfb4* transcripts also fell (Figure 3B). As assessed by ELISA, TGFβ1 exposure was also associated with decreased concentrations of BMP4 and IGFBP4 proteins in media conditioned by MCs (Figure 3C).

Exogenous BMP4 or IGFBP4 ameliorate TGFβ1-induced MMT in vitro

We hypothesised that the diminished levels of BMP4 and IGFBP4 described above might modulate TGFβ1-induced MMT. We administered 50 ng/ml BMP4 or IGFBP4 recombinant proteins to MC cultures. As assessed by gross morphology and immunostaining for ZO1, cingulin and αSMA, addition of either protein alone did not affect the phenotype of these cells (data not shown). In contrast, addition of either BMP4 or IGFBP4 to TGFβ1-exposed cells (Figure 4A) retained aspects of the epithelial phenotype and ameliorated the mesenchymal phenotype as assessed by:

preservation of a cobblestone appearance; a less prominent ZO1 cytoplasmic localisation; and reduction of αSMA immunostaining (Figure 4A), confirmed to be significant upon quantification (Figure 4B). In contrast, neither exogenous BMP4 nor IGFBP4 prevented the loss of cell-cell cingulin localisation following addition of TGFβ1 (Figure 4A). A key event during MMT is cell migration, so we studied this with a scratch assay in MC cultures (Figure 4C). *Versus* controls, MCs exposed to 1 ng/ml TGFβ1 displayed significantly enhanced wound closure at 16 h, consistent with an increased migration. Addition of IGFBP4 or BMP4 significantly limited this effect (Figure 4D).

Exploration of BMP4 in two mouse models of peritoneal fibrosis

In a mouse model of peritoneal fibrosis induced by intraperitoneal TGFβ1-expressing adenovirus, there was an attenuation of BMP4 immunostaining of the surface of the peritoneum (Figure 5A). Next, we 'genetically labelled' peritoneal MCs by activation of the *LacZ* allele induced by activating *Wt1* promoter-driven Cre recombinase. Here, labelled cells and their progeny express a reporter that can be detected using the X-gal reaction. As noted by Lua *et al*. Wt1 promoter-driven Cre recombinase activation occurs in a subset of MCs, so only the fates of the labelled population can be tracked [18]. Mice underwent surgery to induce adhesion formation and a subset were administered BMP4. In whole mount preparations, we found elongated blue cells in zones immediately adjacent to the nascent scar whereas, in injured mice exposed to exogenous BMP4, clusters of cuboidal cells were noted (Figure 5B, upper frames). On histology, cells expressing the reporter were noted under the peritoneal surface after injury whereas, after administration of BMP4, labelled cells were present on the

peritoneal surface (Figure 5B, lower frames). These observations suggest that BMP4 helps restore 'healthy' mesothelial morphology following injury *in vivo*.

Altered patterns of BMP4 and IGFBP4 in human peritoneal dialysis tissue

Mesothelium was identified in control and peritoneal dialysis exposed human peritoneal tissue sections, as determined by HBME1 immunostaining (Figure 6). Control peritoneal tissue, from otherwise healthy patients undergoing incidental hernia surgical repair, showed positive immunostaining for both IGFBP4 and BMP4 on the peritoneal surface. This pattern was attenuated in tissue harvested from peritoneal dialysis patients (Figure 6). Scattered cells below the mesothelial layer showed positive staining for IGFBP4, which may represent retention of some mesothelial characteristics in cells undergoing MMT [10] .

Discussion

Previous studies investigating peritoneal MCs generally analysed cultures obtained solely by enzymatic digestion of omentum [23,33,34]. A few studies have enriched for MCs using procedures such as positive selection for HBME1 using FACS [15], removal of CD45-positive cells [35], or sorting for glycoprotein M6a (GpM6a) expressing cells using magnetic beads [18]. We found similar levels of MC enrichment by FACS or magnetic bead sorting: both use positive sorting with HBME1 antibody against a microvillus protein characteristic of MCs and produced populations in which around 90% of cells were Wt1+. Magnetic bead sorting offers a convenient method which bypasses the need to access cell sorting facilities. Whether sorting using both HBME1 plus another specific MCs marker, such as mesothelin or GpM6a, generates a greater enrichment could be addressed in future studies.

Using RNA sequencing, we identified numerous '*epithelial marker*' RNAs in purified rat MCs, including transcripts encoding ZO1, mesothelin, uroplakin 3B, and podoplanin, similar to previous reports. Purified MCs also expressed high transcript levels for several keratins, for *Wt1*, and for *Msln* encoding the cell-surface protein mesothelin [26]. MCs appear to share certain molecules, including Wt1 and podocalyxin-like protein 1, with podocytes, specialised epithelia within kidney glomeruli. As for podocytes, the molecular signature of MCs has certain similarities to generic mesenchymal cells; for example, both epithelia contain abundant vimentin [36]. Thus, MCs are 'epithelial-like' rather than exactly like 'classic' epithelia.

The expression of the cell-cell junction protein, E-cadherin and its downregulation during EMT reflecting the destabilization of adherens junctions, has been considered a hallmark of EMT and has been noted in some MMT studies [23,35,37]. In our study, however, RNA sequencing of HBME1-sorted rat MCs revealed very low reads for *Cdh1*, the transcript encoding E-cadherin; moreover, there was no significant change after TGFβ1 exposure. Furthermore, E-cadherin was not detected in rat omentum using immunohistochemistry. Notably, literature already points to a heterogeneity of E-cadherin expression by MCs studied in different contexts. Cells harvested from human omentum, or collected from dialysis effluent, expressed E-cadherin [35] but MCs covering the liver [38] or the body wall [18] of mice did not express E-cadherin *in vivo*, nor did human ovarian MCs [39].

Given the heterogeneity of MCs, depending on their source, there are unlikely to be exactly the same changes in gene expression as they undergo MMT. Ruiz-Carpio *et al,* [35] analysed human peritoneal cells that had undergone, or were undergoing, MMT. MMT was associated with increased levels of transcripts for *THBS1*, *VCAN* and *ITGA11,* while *BMP4* and *THBD* were downregulated. Inspection of our RNA sequencing data (ArrayExpress repository E-MTAB-5998 and Tables in this paper) revealed similar significant changes. On the other hand, they noted markedly increased levels of *IL33* and *IL6*, whereas we found that the former transcript was expressed but unchanged after TGFβ1, and the latter was not expressed. Moreover, Ruiz-Carpio *et al*. also noted marked decreased levels of transcripts for *AQP1*, *MUC16* and *VTN*. In our arrays, the former two transcripts were expressed but unchanged by TGFβ1 while the latter was not expressed. Moreover, because MCs are not typical epithelia, MMT molecular profiles are unlikely to be exactly the same

as for EMT. In our RNA-seq study, *Snai1, Snai2* and *Zeb2* were all significantly upregulated in TGFβ1-induced MMT, and all three molecules tend to increase in typical EMT. Conversely, we did not detect TGFβ1-induced changes in either *Cdh2*, encoding the cell-cell junction protein N-cadherin, or in *Twist1* and *Twist2*, encoding transcription factors: all three have been implicated in typical EMT. Collectively, these observations support the idea that that there are unlikely to be exactly the same changes in gene expression in all forms of EMT or MMT.

In the current study, *Sox9* transcripts, encoding sex-determining region Y-box 9, were significantly upregulated in MMT. This transcription factor has been implicated in fibrosis [40] and likely synergizes with SNAIL1 or SNAIL2 to drive EMT [41,42]. The role of Sox9 in regulating MMT and peritoneal fibrosis warrants further investigation. Wt1 is a transcription factor that regulates the balance between EMT and MET in development [43,44]. In the current study, purified MCs expressed high levels of *Wt1* but these showed no significant change in response to TGFβ1. Another group, analysing pleural MCs, detected MMT when Wt1 was experimentally downregulated [45]. Thus, downregulation of Wt1 can be associated with MMT but appears not essential for TGFβ1-induced MMT in our current study.

We also found that TGFβ1 exposure led to an upregulation of transcripts encoding tenascins C and N. Tenascin C is an extracellular matrix protein that has been found to inhibit cellular adhesion to fibronectin and recently proposed to be a potential biomarker in peritoneal dialysis associated with poor membrane function [46]. Tenascin N is a member of the tenascin family previously associated with neurite outgrowth and appears not to have been previously highlighted in MMT so is worthy

of further investigations. Upregulation of neural cell adhesion molecule 1 (NCAM-1) has been reported to promote the formation of focal adhesions in mesothelial-derived tumours [47], but a possible functional role in MMT is yet to be elucidated. Vascular cell adhesion molecule 1 (VCAM-1), important for leucocyte adhesion, was also induced by TGFβ1 and previously reported to be upregulated in MCs exposed to advanced glycation end products [48,49], and the soluble form was reported to inhibit MMT [50].

We hypothesised that if the molecular signature of MMT could be better defined, these insights could then be exploited to functionally block this pathological cellular transition. We discovered that, in response to TGFβ1, MCs showed robust down-regulation of BMP4. Apart from BMP1 which is a metalloprotease, BMPs are growth factors belonging to the TGFβ superfamily that are secreted and bind to dimers of BMP receptors I and II, eliciting intracellular signalling *via* SMAD phosphorylation. BMP4 is required for gastrulation and for lung, heart and kidney development [51]. We reasoned that the TGFβ1-induced depletion of BMP4 might itself modulate MMT. Indeed, recombinant BMP4 partially prevented TGFβ1-induced MMT, as evidenced by retention of membranous ZO1 localisation, lack of αSMA induction and reduced cell migration *in vitro*. Moreover, we found that BMP4 immunostaining on peritoneal surfaces was attenuated *versus* healthy controls in human peritoneal dialysis tissue and in a mouse model of TGFβ1-induced peritoneal fibrosis. Finally, genetic lineage tracing of MCs was used in mice with peritoneal injury. Here, BMP4 administration ameliorated injury-induced shape change and migration of cells expressing the reporter gene. We interpret these results as showing that genetically labelled MCs, and/or their progeny, move under the surface of the injured mesothelium, as also

concluded by Lua *et al*. when they examined a model of chlorhexidine gluconate (CG)-induced fibrosis [18]. Our findings demonstrate a distinctive MMT signature and highlight the therapeutic potential for BMP4 to reduce MMT. Future experiments will be needed, however, to determine whether BMP4 ameliorates the degree of scarring *in vivo*. Although this is a novel finding with regard to MMT, application of BMP4 was shown to reduce retinal epithelial cell EMT in a similar manner [52]. BMP7 has been shown to ameliorate MMT in previous studies, and BMP7 and BMP4 signal though similar pathways [53]. Our RNA sequencing data showed that *Bmp4* was highly expressed in rat MCs whereas *Bmp7* reads were low; moreover only *Bmp4* was significantly downregulated upon exposure to exogenous TGFβ1 (*Bmp4* average reads of 3434 reducing to 1428 with exposure to TGFβ1 (P=5.09E-24); and average *Bmp7* reads at baseline of 80, and 39 upon exposure to exogenous TGFβ1 (P=0.108). Therefore, of these two BMP molecules, it is BMP4 that is the key endogenous factor in our model. In parallel with the downregulation of BMP4 in MCs undergoing MMT, there was an increase in transcripts encoding gremlin-2, a member of the BMP-antagonist gremlin family [29,54]. Notably, it has been reported that adenovirus-mediated upregulation of *gremlin1* promotes peritoneal fibrosis in mice [55]. We speculate that BMP4 signalling *via* phosphorylation of Smad1/5/8 opposes TGFβ1 mediated phosphorylation of Smad2/3 signalling [53]. Thus, the two signalling pathways may keep the balance of homeostasis in the mesothelium.

Our transcriptome analyses also revealed that transcripts encoding growth factors IGF1 and IGF2 were up-regulated during MMT. In parallel, levels of transcripts encoding of IGFBP4 and IGFBP5 were markedly downregulated. These changes are predicted to lead to an increase in IGF signalling activity as IGFBPs lengthen the

half-life of circulating IGF-I due to their higher affinity to IGF ligands than the receptors [31]. We showed that recombinant IGFBP4, like BMP4, ameliorated TGFβ1-induced MMT *in vitro*. Furthermore, immunostaining for IGFBP4 of peritoneal tissues harvested from peritoneal dialysis patients was less prominent in the mesothelial layer with some evidence of expression in cells of the submesothelium that might represent migrated MCs or their progeny. Studies show that IGF signalling interacts at several levels with various components of the TGFβ signalling pathway [56]. In future, it will be important to determine whether similar interactions may be regulating IGF-induced MMT in the peritoneum.

Blocking downstream TGFβ1 signalling pathways may be another way to attenuate MMT including targeting Smad-dependent pathways [57] and Smad-independent such as Akt/mTOR [57], c-Jun N-terminal kinase (JNK)[57], Wnt/β-catenin [58], integrin-linked kinase/glycogen synthase kinase-3β (ILK/GSK-3β) [59], extracellular signal-regulated kinase/nuclear factor kappa B (ERK/NF-κB) [33], and mitogen-activated protein kinase (MAPK) [60]. Another approach, however, based on the findings from the current study, would be to focus on introducing BMP4 and IGFBP4 to prevent MMT and peritoneal fibrosis. Importantly, evidence suggests MMT occurs in diverse peritoneal pathologies including surgical adhesions [61], endometriosis [62] and peritoneal metastasis [63]. Interestingly, in a rat model of surgical adhesions, IGFBP4 administration ameliorated peritoneal scarring [64], although a link to MMT was not explored. Future studies are required to elucidate whether therapeutically manipulating BMP4 or IGFBP4 signalling could ameliorate the severity of these conditions.

Acknowledgements

The Bioimaging Facility microscopes used in this study were purchased with grants from BBSRC, Wellcome and the University of Manchester Strategic Fund. Special thanks goes to Peter March, Roger Meadows and Steven Marsden for their help with the microscopy. We would like to thank Raymond Hodgkiss for technical assistance. We thank Dr Zia Moinuddin (Manchester Royal Infirmary) for collection of human tissue and Dr Peter Margetts (McMaster University, Hamilton, Canada) for AdTGFβ1. This research was supported by Medical Research Council (MR/M012751/1) and Kidneys for Life (1/2016) project grants.

Author contributions

SN contributed to conception and design, all aspects of data acquisition apart from the lineage tracing experiment, and the preparation of figures and drafting the manuscript. SH and AW contributed to conception and design, data interpretation and drafting the manuscript. TW and BW designed and undertook the lineage tracing experiment and revised the manuscript critically. LZ contributed to RNA sequencing data acquisition and preparation of figures. All authors were responsible for approval of the final manuscript.

References

1. Kalluri R, Weinberg RA. The basics of epithelial-mesenchymal transition. *J Clin Invest* 2009; **119**: 1420-1428.
2. Kovacic JC, Mercader N, Torres M*, et al.* Epithelial-to-mesenchymal and endothelial-to-mesenchymal transition: from cardiovascular development to disease. *Circulation* 2012; **125**: 1795-1808.
3. Mutsaers SE, Birnie K, Lansley S*, et al.* Mesothelial cells in tissue repair and fibrosis. *Front Pharmacol* 2015; **6**: 113.
4. Wilm B, Ipenberg A, Hastie ND*, et al.* The serosal mesothelium is a major source of smooth muscle cells of the gut vasculature. *Development* 2005; **132**: 5317-5328.
5. Que J, Wilm B, Hasegawa H*, et al.* Mesothelium contributes to vascular smooth muscle and mesenchyme during lung development. *Proc Natl Acad Sci U S A* 2008; **105**: 16626-16630.
6. Lamouille S, Xu J, Derynck R. Molecular mechanisms of epithelial-mesenchymal transition. *Nat Rev Mol Cell Biol* 2014; **15**: 178-196.
7. Thiery JP, Sleeman JP. Complex networks orchestrate epithelial-mesenchymal transitions. *Nat Rev Mol Cell Biol* 2006; **7**: 131-142.
8. Flier SN, Tanjore H, Kokkotou EG*, et al.* Identification of epithelial to mesenchymal transition as a novel source of fibroblasts in intestinal fibrosis. *J Biol Chem* 2010; **285**: 20202-20212.
9. Yang AH, Chen JY, Lin JK. Myofibroblastic conversion of mesothelial cells. *Kidney Int* 2003; **63**: 1530-1539.

10. Yanez-Mo M, Lara-Pezzi E, Selgas R, *et al.* Peritoneal dialysis and epithelial-to-mesenchymal transition of mesothelial cells. *N Engl J Med* 2003; **348**: 403-413.

11. Strippoli R, Benedicto I, Perez Lozano ML, *et al.* Inhibition of transforming growth factor-activated kinase 1 (TAK1) blocks and reverses epithelial to mesenchymal transition of mesothelial cells. *PLoS One* 2012; **7**: e31492.

12. Fang CC, Huang JW, Shyu RS, *et al.* Fibrin-Induced epithelial-to-mesenchymal transition of peritoneal mesothelial cells as a mechanism of peritoneal fibrosis: effects of pentoxifylline. *PLoS One* 2012; **7**: e44765.

13. LeBleu VS, Taduri G, O'Connell J, *et al.* Origin and function of myofibroblasts in kidney fibrosis. *Nat Med* 2013; **19**: 1047-1053.

14. Foley-Comer AJ, Herrick SE, Al-Mishlab T, *et al.* Evidence for incorporation of free-floating mesothelial cells as a mechanism of serosal healing. *J Cell Sci* 2002; **115**: 1383-1389.

15. Lansley SM, Searles RG, Hoi A, *et al.* Mesothelial cell differentiation into osteoblast- and adipocyte-like cells. *J Cell Mol Med* 2011; **15**: 2095-2105.

16. Margetts PJ, Hoff C, Liu L, *et al.* Transforming growth factor beta-induced peritoneal fibrosis is mouse strain dependent. *Nephrol Dial Transplant* 2013; **28**: 2015-2027.

17. Gorvy DA, Herrick SE, Shah M, *et al.* Experimental manipulation of transforming growth factor-beta isoforms significantly affects adhesion formation in a murine surgical model. *Am J Pathol* 2005; **167**: 1005-1019.

18. Lua I, Li Y, Pappoe LS, *et al.* Myofibroblastic Conversion and Regeneration of Mesothelial Cells in Peritoneal and Liver Fibrosis. *Am J Pathol* 2015; **185**: 3258-3273.

19. Aguilera A, Yanez-Mo M, Selgas R*, et al.* Epithelial to mesenchymal transition as a triggering factor of peritoneal membrane fibrosis and angiogenesis in peritoneal dialysis patients. *Curr Opin Investig Drugs* 2005; **6**: 262-268.

20. Loureiro J, Aguilera A, Selgas R*, et al.* Blocking TGF-beta1 protects the peritoneal membrane from dialysate-induced damage. *J Am Soc Nephrol* 2011; **22**: 1682-1695.

21. Chen YT, Chang YT, Pan SY*, et al.* Lineage tracing reveals distinctive fates for mesothelial cells and submesothelial fibroblasts during peritoneal injury. *J Am Soc Nephrol* 2014; **25**: 2847-2858.

22. Xiao L, Peng X, Liu F*, et al.* AKT regulation of mesothelial-to-mesenchymal transition in peritoneal dialysis is modulated by Smurf2 and deubiquitinating enzyme USP4. *BMC Cell Biol* 2015; **16**: 7.

23. Jin X, Ren S, Macarak E*, et al.* Pathobiological mechanisms of peritoneal adhesions: The mesenchymal transition of rat peritoneal mesothelial cells induced by TGF-beta1 and IL-6 requires activation of Erk1/2 and Smad2 linker region phosphorylation. *Matrix Biol* 2016; **51**: 55-64.

24. Retana C, Sanchez E, Perez-Lopez A*, et al.* Alterations of intercellular junctions in peritoneal mesothelial cells from patients undergoing dialysis: effect of retinoic Acid. *Perit Dial Int* 2015; **35**: 275-287.

25. Kanamori-Katayama M, Kaiho A, Ishizu Y*, et al.* LRRN4 and UPK3B are markers of primary mesothelial cells. *PLoS One* 2011; **6**: e25391.

26. Ma J, Tang WK, Esser L*, et al.* Recognition of mesothelin by the therapeutic antibody MORAb-009: structural and mechanistic insights. *J Biol Chem* 2012; **287**: 33123-33131.

27. Medina A, Ghaffari A, Kilani RT*, et al.* The role of stratifin in fibroblast-keratinocyte interaction. *Mol Cell Biochem* 2007; **305**: 255-264.

28. Mladinich M, Ruan D, Chan CH. Tackling Cancer Stem Cells via Inhibition of EMT Transcription Factors. *Stem Cells Int* 2016; **2016**: 5285892.

29. Yeung CY, Gossan N, Lu Y*, et al.* Gremlin-2 is a BMP antagonist that is regulated by the circadian clock. *Sci Rep* 2014; **4**: 5183.

30. Vadon-Le Goff S, Hulmes DJ, Moali C. BMP-1/tolloid-like proteinases synchronize matrix assembly with growth factor activation to promote morphogenesis and tissue remodeling. *Matrix Biol* 2015; **44-46**: 14-23.

31. Duan C, Xu Q. Roles of insulin-like growth factor (IGF) binding proteins in regulating IGF actions. *Gen Comp Endocrinol* 2005; **142**: 44-52.

32. Monget P, Oxvig C. PAPP-A and the IGF system. *Ann Endocrinol (Paris)* 2016; **77**: 90-96.

33. Strippoli R, Benedicto I, Perez Lozano ML*, et al.* Epithelial-to-mesenchymal transition of peritoneal mesothelial cells is regulated by an ERK/NF-kappaB/Snail1 pathway. *Dis Model Mech* 2008; **1**: 264-274.

34. Liu FY, Duan SB, Long ZG. [Culture and characterization of human peritoneal mesothelial cells]. *Hunan Yi Ke Da Xue Xue Bao* 2001; **26**: 321-324.

35. Ruiz-Carpio V, Sandoval P, Aguilera A*, et al.* Genomic reprograming analysis of the Mesothelial to Mesenchymal Transition identifies biomarkers in peritoneal dialysis patients. *Sci Rep* 2017; **7**: 44941.

36. May CJ, Saleem M, Welsh GI. Podocyte dedifferentiation: a specialized process for a specialized cell. *Front Endocrinol (Lausanne)* 2014; **5**: 148.

37. Lopez-Cabrera M. Mesenchymal Conversion of Mesothelial Cells Is a Key Event in the Pathophysiology of the Peritoneum during Peritoneal Dialysis. *Adv Med* 2014; **2014**: 473134.

38. Li Y, Wang J, Asahina K. Mesothelial cells give rise to hepatic stellate cells and myofibroblasts via mesothelial-mesenchymal transition in liver injury. *Proc Natl Acad Sci U S A* 2013; **110**: 2324-2329.

39. Auersperg N, Pan J, Grove BD*, et al.* E-cadherin induces mesenchymal-to-epithelial transition in human ovarian surface epithelium. *Proc Natl Acad Sci U S A* 1999; **96**: 6249-6254.

40. Hanley KP, Oakley F, Sugden S*, et al.* Ectopic SOX9 mediates extracellular matrix deposition characteristic of organ fibrosis. *J Biol Chem* 2008; **283**: 14063-14071.

41. Sakai D, Suzuki T, Osumi N*, et al.* Cooperative action of Sox9, Snail2 and PKA signaling in early neural crest development. *Development* 2006; **133**: 1323-1333.

42. Kondoh H, Kamachi Y. SOX-partner code for cell specification: Regulatory target selection and underlying molecular mechanisms. *Int J Biochem Cell Biol* 2010; **42**: 391-399.

43. von Gise A, Zhou B, Honor LB*, et al.* WT1 regulates epicardial epithelial to mesenchymal transition through beta-catenin and retinoic acid signaling pathways. *Dev Biol* 2011; **356**: 421-431.

44. Plones T, Fischer M, Hohne K*, et al.* Turning back the Wheel: Inducing Mesenchymal to Epithelial Transition via Wilms Tumor 1 Knockdown in Human Mesothelioma Cell Lines to Influence Proliferation, Invasiveness, and Chemotaxis. *Pathol Oncol Res* 2017.

45. Karki S, Surolia R, Hock TD*, et al.* Wilms' tumor 1 (Wt1) regulates pleural mesothelial cell plasticity and transition into myofibroblasts in idiopathic pulmonary fibrosis. *FASEB J* 2014; **28**: 1122-1131.

46. Hirahara I, Kusano E, Imai T*, et al.* Effluent Tenascin-C Levels Reflect Peritoneal Deterioration in Peritoneal Dialysis: MAJOR IN PD Study. *Biomed Res Int* 2015; **2015**: 241098.

47. Zecchini S, Bombardelli L, Decio A*, et al.* The adhesion molecule NCAM promotes ovarian cancer progression via FGFR signalling. *EMBO Mol Med* 2011; **3**: 480-494.

48. Boulanger E, Wautier MP, Wautier JL*, et al.* AGEs bind to mesothelial cells via RAGE and stimulate VCAM-1 expression. *Kidney Int* 2002; **61**: 148-156.

49. Cook-Mills JM, Marchese ME, Abdala-Valencia H. Vascular cell adhesion molecule-1 expression and signaling during disease: regulation by reactive oxygen species and antioxidants. *Antioxid Redox Signal* 2011; **15**: 1607-1638.

50. Dokic D, Dettman RW. VCAM-1 inhibits TGFbeta stimulated epithelial-mesenchymal transformation by modulating Rho activity and stabilizing intercellular adhesion in epicardial mesothelial cells. *Dev Biol* 2006; **299**: 489-504.

51. Jiao K, Kulessa H, Tompkins K*, et al.* An essential role of Bmp4 in the atrioventricular septation of the mouse heart. *Genes Dev* 2003; **17**: 2362-2367.

52. Yao H, Li H, Yang S*, et al.* Inhibitory Effect of Bone Morphogenetic Protein 4 in Retinal Pigment Epithelial-Mesenchymal Transition. *Sci Rep* 2016; **6**: 32182.

53. Salazar VS, Gamer LW, Rosen V. BMP signalling in skeletal development, disease and repair. *Nat Rev Endocrinol* 2016; **12**: 203-221.

54. Sun J, Zhuang FF, Mullersman JE*, et al.* BMP4 activation and secretion are negatively regulated by an intracellular gremlin-BMP4 interaction. *J Biol Chem* 2006; **281**: 29349-29356.

55. Siddique I, Curran SP, Ghayur A*, et al.* Gremlin promotes peritoneal membrane injury in an experimental mouse model and is associated with increased solute transport in peritoneal dialysis patients. *Am J Pathol* 2014; **184**: 2976-2984.

56. Danielpour D, Song K. Cross-talk between IGF-I and TGF-beta signaling pathways. *Cytokine Growth Factor Rev* 2006; **17**: 59-74.

57. Patel P, Sekiguchi Y, Oh KH*, et al.* Smad3-dependent and -independent pathways are involved in peritoneal membrane injury. *Kidney Int* 2010; **77**: 319-328.

58. Zhang F, Liu H, Liu F*, et al.* New insights into the pathogenesis and treatment of peritoneal fibrosis: a potential role of Wnt/beta-catenin induced epithelial to mesenchymal transition and stem cells for therapy. *Med Hypotheses* 2013; **81**: 97-100.

59. Luo L, Liu H, Dong Z*, et al.* Small interfering RNA targeting ILK inhibits EMT in human peritoneal mesothelial cells through phosphorylation of GSK3beta. *Mol Med Rep* 2014; **10**: 137-144.

60. Jang YH, Shin HS, Sun Choi H*, et al.* Effects of dexamethasone on the TGF-beta1-induced epithelial-to-mesenchymal transition in human peritoneal mesothelial cells. *Lab Invest* 2013; **93**: 194-206.

61. Sandoval P, Jimenez-Heffernan JA, Guerra-Azcona G*, et al.* Mesothelial-to-mesenchymal transition in the pathogenesis of post-surgical peritoneal adhesions. *J Pathol* 2016; **239**: 48-59.

62. Demir AY, Demol H, Puype M*, et al.* Proteome analysis of human mesothelial cells during epithelial to mesenchymal transitions induced by shed menstrual effluent. *Proteomics* 2004; **4**: 2608-2623.

63. Rynne-Vidal A, Au-Yeung CL, Jimenez-Heffernan JA*, et al.* Mesothelial-to-mesenchymal transition as a possible therapeutic target in peritoneal metastasis of ovarian cancer. *J Pathol* 2017; **242**: 140-151.

64. Gimbel ML, Chelius D, Hunt TK*, et al.* A novel approach to reducing postoperative intraperitoneal adhesions through the inhibition of insulinlike growth factor I activity. *Arch Surg* 2001; **136**: 311-317.

65. Soriano P. Generalized lacZ expression with the ROSA26 Cre reporter strain. *Nat Genet* 1999; **21**: 70-71.

66. Zhou B, Ma Q, Rajagopal S*, et al.* Epicardial progenitors contribute to the cardiomyocyte lineage in the developing heart. *Nature* 2008; **454**: 109-113.

67. Wilm B, Munoz-Chapuli R. Tools and Techniques for Wt1-Based Lineage Tracing. *Methods Mol Biol* 2016; **1467**: 41-59.

68. Sulaiman H, Gabella G, Davis C*, et al.* Growth of nerve fibres into murine peritoneal adhesions. *J Pathol* 2000; **192**: 396-403.

Tables

Table 1. Epithelial signature transcripts

Gene Symbol	Encoded molecule	Control mean reads	TGFβ1 mean reads	log2Fold Change (paired)	FDR
Down-regulated genes					
Cgn	Cingulin	1559	560	-1.507	2.03E-26
Podxl	Podocalyxin-like	6607	3107	-1.163	1.09E-11
Cldn15	Claudin 15	9166	5886	-0.654	1.14E-09
Cldn2	Claudin 2	1427	781	-0.797	4.41E-08
Col4a3	Collagen 2C type IV	488	248	-1.186	2.38E-07
Upk3b	Uroplakin 3B	20429	14864	-0.467	3.73E-06
Col4a4	Collagen 2C_type_IV 2C_alpha_4	11887	5809	-1.265	4.03E-06
Krt23	Keratin_23	135	48	-1.388	5.08E-06
Krt13	Keratin_13	426	217	-1.250	6.08E-06
Tjp1	Tight_junction_protein_1 (ZO-1)	15384	11569	-0.416	3.38E-05
Itgb3	Integrin_subunit_beta_3	689	396	0.682	9.00E-05
Ppl	Periplakin	5588	2588	-1.160	0.000133
Itga6	Integrin_subunit_alpha_6	1325	774	-0.842	0.000297
Lamb2	Laminin_subunit_beta_2	6366	4755	-0.423	0.001374
Itgb4	Integrin_subunit_beta_4	1367	975	-0.500	0.001535
Krt19	Keratin_19	463	216	-1.581	0.00259
Krt18	Keratin_18	350	232	-0.727	0.002744
Lamb3	Llaminin_subunit_beta_3	35	13	-1.399	0.007653
Cldn1	Claudin_1	5787	4347	-0.445	0.015106
Krtap17-1	Keratin_associated_protein_17-1	12	2	-2.480	0.033379
Lyve1	Lymphatic_vessel_endothelial_hyaluronan_receptor_1	1279	233	-1.514	0.036201
Unaltered genes					
Cdh1	Cadherin_1	20	26	0.673	0.441269
Wt1	Wilms_tumor_1	10613	10041	-0.091	0.588825
Msln	Mesothelin	63897	62175	-0.046	0.8759
Up-regulated genes					
Sfn	Stratifin	66	472	2.802	1.53E-33
Lamc2	Laminin_subunit_gamma_2	180	245	0.450	0.014634

Selected 'epithelial' transcripts, with mean number of reads in control and TGFβ1 exposed MCs, along with log2fold change and P values corrected for false discovery rate (FDR).

Table 2. Mesenchymal/Extracellular matrix transcripts

Gene Symbol	Encoded molecule	Control mean reads	TGFβ1 mean reads	log2Fold Change (paired)	FDR
Up-regulated genes					
Ncam1	Neural_cell_adhesion_molecule_1	3953	12859	1.697	5.70E-86
Vcam1	Vascular_cell_adhesion_molecule_1	228	1520	2.655	1.76E-54
Tnc	Tenascin_C	2051	23742	3.411	1.10E-24
Myh10	Myosin 2C_heavy_chain_10 2C_non-muscle	11788	18601	0.657	8.78E-24
Tnn	Tenascin_N	36	1107	4.501	8.21E-21
Col4a1	Collagen 2C_type_IV 2C_alpha_1	77636	135323	0.846	5.64E-19
Itga8	Integrin_subunit_alpha_8	3040	7398	1.261	4.60E-18
Vcl	Vinculin	5691	9826	0.776	8.38E-16
Fscn1	Fascin_actin-bundling_protein_1	1041	2146	1.043	5.51E-13
Col4a2	Collagen 2C_type_IV 2C_alpha_2	46061	67902	0.587	2.61E-12
Col5a1	Collagen 2C_type_V 2C_alpha_1	32014	53822	0.714	2.27E-11
Nexn	Nexilin_(F_actin_binding_protein)	168	474	1.521	2.76E-11
Msn	Moesin	15597	24472	0.649	2.60E-10
Col1a1	Collagen 2C_type_I 2C_alpha_1	394092	603398	0.614	6.44E-10
Tns1	Tensin_1	10590	14483	0.456	9.23E-10
Vim	Vimentin	44279	68467	0.607	5.02E-09
Myh11	Myosin 2C_heavy_chain_11 2C_smooth_muscle	302	797	1.225	8.56E-08
Tagln	Transgelin	12509	47656	1.871	1.13E-07
Itga11	Iintegrin_subunit_alpha_11	457	1006	0.987	6.25E-07
Col5a2	Collagen 2C_type_V%2C_alpha_2	82389	108911	0.401	3.98E-06
Itgb1	Integrin_subunit_beta_1	78702	105859	0.415	1.32E-05
Acta1	Actin 2C_alpha_1 2C_skeletal_muscle	5	41	2.685	3.50E-05
Itga5	Integrin_subunit_alpha_5	4444	6242	0.497	0.000182
Vcan	Versican	4112	7823	1.073	0.000438
Itgae	Integrin_subunit_alpha_E	147	228	0.629	0.00048
Itgb6	Integrin_subunit_beta_6	10	32	1.673	0.001715
Col3a1	Collagen 2C_type_III 2C_alpha_1	378113	468616	0.303	0.001948
Des	Desmin	5410	6856	0.347	0.002501
Acta2	Actin 2C_alpha_2 2C_smooth_muscle 2C_aorta (α-sma)	5648	22466	1.970	0.003539
Cib2	Calcium_and_integrin_binding_family_member_2	235	337	0.514	0.006403
Itgav	Integrin_subunit_alpha_V	3648	4592	0.351	0.013587
Itga10	Integrin_subunit_alpha_10	3	14	2.126	0.01948
Itgbl1	Integrin_subunit_beta_like_1	5767	7379	0.389	0.021021
Itga1	Integrin_subunit_alpha_1	794	1035	0.382	0.03803
Unaltered genes					
F13a1	Coagulation_factor_XIII_A1_chain	3158	818	-1.105	0.125258
Cdh2	Cadherin_2	4330	4467.3	0.014	0.979014
Down-regulated genes					
S100a4	S100_calcium-binding_protein_A4 (FSP1)	10232	6267	-0.730	1.33E-11

Selected ‘mesenchymal’ and extracellular matrix molecule transcripts, with mean number of reads in control and TGFβ1 exposed MCs, along with log2 fold change and P values corrected for false discovery rate (FDR).

Table 3. Transcription and growth factors previously implicated in EMT and/or MMT

Gene Symbol	Encoded molecule	Control mean reads	TGFβ1 mean reads	log2Fold Change (paired)	FDR
Up-regulated genes					
Postn	Periostin	907	12663	3.933	4.53E-37
Tgfb2	Transforming_growth_factor 2C_beta_2	1168	2590	1.123	1.17E-23
Wisp1	WNT1_inducible_signaling_pathway_protein_1	2311	3982	0.803	8.75E-17
Mmp2	Matrix_metallopeptidase_2	8079	13357	0.694	9.05E-16
Timp1	TIMP_metallopeptidase_inhibitor_1	6227	10470	0.710	7.29E-13
Wnt5a	Wingless-type_MMTV_integration_site_family 2C_member_5A	1322	2643	0.966	9.07E-13
Snai1	Snail_family_transcriptional_repressor_1	733	1275	0.757	2.66E-11
Tgfb1i1	Transforming_growth_factor_beta_1_induced_transcript_1	1173	2006	0.794	1.61E-08
Wnt2	Wingless-type_MMTV_integration_site_family_member_2	261	442	0.737	8.48E-08
Tgfb1	Transforming_growth_factor 2C_beta_1	798	1285	0.677	4.76E-07
Fndc3b	Fibronectin_type_III_domain_containing_3B	4264	5293	0.311	7.17E-06
Sparc	Secreted_protein_acidic_and_cysteine_rich	266980	341541	0.355	3.83E-05
Sox9	SRY_box_9	14	92	2.186	4.35E-05
Tgfb3	Transforming_growth_factor 2C_beta_3	8046	11071	0.440	7.64E-05
Snai2	Snail_family_transcriptional_repressor_2	125	232	0.866	7.85E-05
Wnt11	Wingless-type_MMTV_integration_site_family 2C_member_11	290	462	0.771	0.00019
Thbs1	Thrombospondin_1	8482	27041	1.534	0.000224
Mmp19	Matrix_metallopeptidase_19	1735	2187	0.327	0.000827
Zeb2	Zinc_finger_E-box_binding_homeobox_2	1129	1412	0.314	0.000898
Cemip	Cell_migration-inducing_hyaluronan_binding_protein	11610	28004	1.630	0.004018
Plat	Plasminogen_activator 2C_tissue_type	9468	11604	0.304	0.015156
Serpine1	Serpin_family_E_member_1	25951	84335	1.824	0.032918
Unaltered genes					
Twist1	Twist_family_bHLH_transcription_factor_1	246	349	0.488	0.067817
Ctnnb1	Catenin_beta_1	7810	8552	0.131	0.139767
Twist2	Twist_family_bHLH_transcription_factor_2	65	95	0.534	0.17583
Ctnna1	Catenin_alpha_1	7268	7430	0.033	0.979014
Down-regulated genes					
Thbd	Thrombomodulin	3755	1352	-1.451	1.37E-33
Timp4	Tissue_inhibitor_of_metalloproteinase_4	263	118	-1.109	3.41E-08
Wnt2b	Wingless-type_MMTV_integration_site_family 2C_member_2B	6478	4378	-0.606	5.05E-08
Fgf1	Fibroblast_growth_factor_1	11522	6146	-1.101	0.000169
Timp2	TIMP_metallopeptidase_inhibitor_2	40410	30888	-0.375	0.000923
Zeb1	Zinc_finger_E-box_binding_homeobox_1	836	686	-0.288	0.035739

Selected transcripts for growth factors and transcription factors previously implicated in EMT and/or MMT. Table contains mean number of reads in control and TGFβ1 exposed MCs along with log2 fold change and P values corrected for false discovery rate (FDR).

Table 4. Transcripts implicated in BMP and IGF signalling

Gene Symbol	Encoded molecule	Control mean reads	TGFβ1 mean reads	log2Fold Change (paired)	FDR
Up-regulated genes					
Igf1	Insulin-like_growth_factor_1	4217	8274	0.953	1.52E-29
Pappa	Pregnancy-associated_plasma_protein_A	127	414	1.642	2.06E-22
Bmp1	Bone_morphogenetic_protein_1	4437	6267	0.499	1.51E-11
Grem2	Gremlin_2 2C_DAN_family_BMP_antagonist	535	1340	1.297	1.07E-11
Igfbp7	Insulin-like_growth_factor_binding_protein_7	28855	34731	0.269	0.000225
Igf2	Insulin-like_growth_factor_2	62	118	1.437	0.000761
Unaltered genes					
Bmp7	Bone_morphogenetic_protein_7	80	39	-0.929	0.108664
Down-regulated genes					
Igfbp4	Insulin-like_growth_factor_binding_protein_4	14736	3884	-1.951	3.62E-50
Bmp4	Bone_morphogenetic_protein_4	3434	1428	-1.370	5.09E-24
Igfbp6	Insulin-like_growth_factor_binding_protein_6	9830	6109	-0.673	2.20E-12
Igfbp5	Insulin-like_growth_factor_binding_protein_5	22768	9320	-1.454	4.32E-07
Igfbp2	Insulin-like_growth_factor_binding_protein_2	41556	29962	-0.502	2.27E-05

Selected novel transcripts from BMP and IGF signalling pathways implicated in MMT. Table contains mean number of reads in control and TGFβ1 exposed MCs, along with log2 fold change.

List of supplementary files:

1. Supplementary materials and methods.
2. Supplementary figure 1.

Figure legends

Figure 1. Mesothelial cell enrichment using HBME1 as a surface marker. A. Fluorescence microscopy of rat omentum, showing all nuclei stained with DAPI, the mesothelial cell apical surface immunostained for HBME1, followed by merged overlay image. Scale bars are 50 μm. **B.** Phase contrast and immunofluorescence images of primary cultures of unsorted, HBME1-FACS sorted and HBME1-magnetic bead (Mojo) sorted cells; note the prominent cobblestone phenotype of the sorted cells. Scale bars are 200 μm. Relative to unsorted cells, both FACS and Mojo sorted cells give an impression of marked enrichment for HBME1. Note the presence of both Wt1+ (Arrowhead) and Wt1- (Arrow) nuclei in the unsorted population stained with DAPI. Scale bars are 50 μm **C.** Relative to unsorted cells, HBME1 enrichment was confirmed by measuring the pixels of positive immunostaining normalised to DAPI nuclei in FACS sorted (P=0.022) and Mojo sorted cells (P=0.005; n=6; mean±SEM). **D.** The percentage of Wt1+ nuclei was significantly increased following either FACS (P=0.02) or Mojo sorting (P=0.017; n=3; mean±SEM). **E.** Cells were maintained for 48 h in either basal media alone, or media supplemented with 1 ng/ml TGFβ1. Note the disruption of the cobblestone phenotype under TGFβ1 treatment, with cells becoming elongated. Scale bars are 50 μm. **F.** Fluorescence microscopy of cells at 48 h demonstrating that exposure to TGFβ1 was associated with disruption of reticular cell-cell junctional ZO1 pattern with more prominent cytoplasmic immunostaining for vimentin and αSMA. Nuclei stained with DAPI. Scale bars are 50 μm.

Figure 2. Transcriptome analyses of HBME1-sorted rat mesothelial cells. A. Unsupervised hierarchical clustering by transcript expression. Rows are expression levels denoted as the z-score, displayed in a high-low (red-blue) colour scale, numeric scale indicates z-transformation. Note that levels of numerous transcripts are increased or decreased after 48 h of exposure to 1 ng/ml TGFβ1. 'Cntrl' are the five vehicle-only exposed samples. 'TGF' are the five parallel cultures exposed to TGFβ1. **B.** Selected RNA-seq data displayed as a volcano plot with the image annotated for '*epithelial signature'* transcripts. **C.** QPCR for *Cdh1*, *Col4a3*, *Col4a4*, *Cng, Pdxl*, *Snai1, Tjp1*, *Upk3b*, and *Vim* (n=3; mean±SEM).

Figure 3. **MMT is associated with dysregulation of BMP4 and IGF pathways**. **A.** Volcano plot annotated with transcripts encoding molecules implicated in BMP and IGF signalling. **B.** Confirmation of decreased levels of *Bmp4* (P=0.024, n=3; mean±SEM), and *Igfbp4* (P=0.012, n=3; mean±SEM) as assessed by QPCR. **C.** As determined by ELISA, concentrations of BMP4 (P=0.023, n=5; mean±SEM) and IGFBP4 (P=0.019, n=5; mean±SEM) were decreased in media conditioned by cells exposed to 1 ng/ml TGFβ1.

Figure 4. Application of BMP4 or IGFBP4 to TGFβ1-exposed rat mesothelial cells. A. Cells were maintained for 48 h in either basal media alone (Control), media supplemented with 1 ng/ml TGFβ1, or the latter supplemented with either 50 ng/ml of BMP4 (TGFβ1+BMP4) or 50 ng/ml IGFBP4 (TGFβ1+IGFBP4). Cells were imaged by phase contrast (top row) or, as shown in subsequent rows, by immunofluorescence for ZO1, cingulin and αSMA with all nuclei counterstained with DAPI (blue). Note that exposure to either BMP4 or IGFBP4: partially preserved the cobblestone pattern of

the monolayer; ameliorated cytoplasmic localisation of ZO1; and reduced αSMA. In contrast, neither factor rescued the TGFβ1-induced disruption of cingulin. Scale bars are 50 μm. **B.** Quantification of αSMA by immunofluorescence, showing a significantly (P=0.0005, n=5; mean±SEM) increased immunostaining in TGFβ1-treated *versus* control cells. There was a significant reduction of αSMA expression in cells co-treated with TGFβ1+BMP4 (P=0.019) or TGFβ1+IGFBP4 (P=0.036). **C.** Phase contrast images showing mesothelial cell migration into a wound over 16 hours under different conditions. Scale bars are 200 μm. **D**. Quantification of mesothelial cell migration under different conditions (n=6; mean±SEM). Note that TGFβ1 exposure was associated with more extensive migration *versus* control (P=0.010 n=6), and that this effect was abrogated when either BMP4 (P=0.012) or IGFBP4 (P=0.005) was added with TGFβ1.

Figure 5. BMP4 in murine models of peritoneal fibrosis. A. Immunostaining for cytokeratin in the peritoneum of mice showed diminished mesothelial-specific expression in response to TGFβ1 adenovirus (AD) compared with control (AdDL) showing nuclei stained with DAPI. In response to TGFβ1 overexpression, the peritoneum was extensively thickened, as shown by Massons trichrome, with near complete loss of surface BMP4 immunostaining. Scale bars are 100 μm. **B.** Following surgical injury, the peritoneum of *Wt1*-lineage tracing mice was stained with XGal. Cells expressing the *LacZ* reporter gene appear blue and represent the fates of subsets of mesothelial cells and/or their progeny. The top two frames show whole mounts, looking down on the peritoneal surface. Injured mice that received vehicle alone (left frame) had elongated and spindle-shaped labelled cells whereas cobblestone-like cell clusters were seen in similarly-injured mice that had received

BMP4 (right frame). Scale bars are 100μm. The lower two frames show histology of peritoneum, with eosin (pink) counterstaining: the peritoneal surface is at the top. Injured mice receiving vehicle alone (left frame) showed labelled cells (arrows) below the surface (arrowheads) of the peritoneum. In injured mice that had received BMP4 (right frame), labelled cells (arrows) were noted on the surface of the peritoneum. Scale bars are 20μm. Representative images from n=3 in each group.

Figure 6. Human fibrotic tissue displays altered patterns of BMP4 and IGFBP4. Human control peritoneum or thickened peritoneum samples from peritoneal dialysis patients were immunostained for HBME1 to identify mesothelium. Control peritoneum displayed prominent mesothelial IGFBP4 and BMP4 immunostaining which was attenuated in peritoneal dialysis samples. In the peritoneal dialysis samples, scattered IGFBP4+ cells were noted below the peritoneal surface. Scale bar is 100 μm.

Supplementary Information file

Functional molecules in mesothelial-to-mesenchymal transition revealed by transcriptome analyses

Sara Namvar[1,2], Adrian S. Woolf[1,2,3], Leo A.H. Zeef[1,2], Thomas Wilm[4], Bettina Wilm[4] and Sarah E. Herrick[1,2].

[1]Division of Cell Matrix Biology and Regenerative Medicine, School of Biological Sciences, Faculty of Biology Medicine and Health, University of Manchester, UK.

[2]Manchester Academic Health Science Centre, Manchester, UK.

[3]Royal Manchester Children's Hospital, Manchester University NHS Foundation Trust, Manchester, UK.

[4]Institute of Translational Medicine, University of Liverpool, UK.

Supplementary Methods

RNA sequencing (RNA-seq) and quantitative polymerase chain reaction (QPCR)

For RNA-seq, paired samples (n=5) from control and TGFβ1-exposed MCs were collected in RNA protect (Thermo Fisher Scientific) and RNA extracted using the RNeasy Plus Mini Kit (Qiagen, Manchester UK). Libraries were generated with the TruSeq Stranded mRNA Library Prep Kit and sequenced paired-end on the Illumina HiSeq4000 platform with an average of 33 million reads per sample (ArrayExpress repository E-MTAB-5998). Sequences were tested by FastQC v0.11.5 using various metrics (http://www.bioinformatics.babraham.ac.uk/projects/fastqc/). Sequence adapters were removed and reads were quality trimmed using Trimmomatic v0.36 (PMID: 24695404). The reads were mapped against the reference rat genome, rn6 using STAR v2.4.2 (PMID: 23104886). Counts per gene were calculated with HTSeq v0.6.1 (PMID: 25260700) using annotation from Ensembl v6.0.85. Normalisation and differential expression was calculated with DESeq2 v1.10.1, R v3.2.3 (PMID: 25516281). Differentially expressed transcripts were defined as those showing at least a 0.36 log 2 fold increase or decrease *versus* controls, and a statistical significance of $P<0.05$ corrected for multiple comparisons. For QPCR, cDNA was synthesised using the TaqMan Reverse Transcription Reagent kit (Thermo Fisher Scientific). QPCR was performed using the RotorGene 6000 (Qiagen) with 2X SensiFAST SYBRGreen No-ROX (Bioline), cDNA template and rat specific primers (Primerdesign, Eastleigh, UK; Supplementary Material). Data was normalised to the housekeeping transcript *Gapdh* and analysed by the ΔΔCT method. Note that, as assessed by RNA-seq, *Gapdh* levels showed no significant difference between

control and TGFβ1-exposed MCs. The following forward and reverse primers were used:

5'-GACATGCCGCCTGGAGAAAC-3' and 5'-AGCCCAGGATGCCCTTTAGT-3' for Gapdh, 5'-ATTTCTCTGCCTCTTCCAAACTT-3' and 5'-CCGTCTTAATCAGGAGTGTTCTT-3' for Vimentin, 5'-CGCTTCAGCCTTCCTCTCAT-3' and 5'-GCTCCTCTGTGAGTCGTTGT-3' for Podxl, 5'-AACCCGAAACTGATGCTATGG-3' and 5'-CCTTGGAATGTATGTGGAGAGAA-3' for Zo1, 5'-CTCTATCCAGATTGATGATGAACGG-3' and 5'-CTTCTTCCTCAGGCTGTCCAG-3'for Cgn, 5'-CCAAGCGTAGTCCCAAGCA-3' and 5'-GCCACGATCCAATCATTCCAG-3' for Bmp4, 5'-AACACCCTCCCTCTCAATGTG-3' and 5'-GAGGACCTGAGGAATGACCTAC-3' for Igfbp4, 5'-GCCAGGATGTTCCCCAATG-3' and 5'-CGAAAGTGACCGTGCTGTAT-3' for Wt1, 5'-GCTGCCAGGACCAGTGATT-3' and 5'-TGACCATAGGAGTCTCCAGGT-3' for Col4a3, 5-'AACTCGCAGCCAGCACAC-3' and 5'-CAGAAGATTCTCATGGACAGTTGG-3' for Col4a4, 5-'ATGACACCATCTGGCTAGTGG-3' and 5'-ATCTTAGCAGCGGTCTGTGG-3' for Up3b and CATGAGTGTCCCCCGGTATC-3' AND 5'-CAGTATCAGCCGCTTTCAGA for Cdh1.

Immunostaining rat tissues

Cells were cultured on glass chamber slides (ThermoFisher). PFA-fixed cultures were incubated for 30 min at room temperature with primary antibodies to: α-smooth muscle actin (α-SMA 1:400; Sigma Aldrich); cingulin (1:100; Thermofisher); E-cadherin (ab76055 Abcam 1:50 or BD610181 BD Biosciences 1:250) **;** HBME1 (1:50; Dako); vimentin (1:100; Sigma Aldrich); Wilms tumour 1 (Wt1; 1:100; Heidelberg, Germany); or zonula occludens 1 (ZO1; 1:50; Thermofisher). For E-

cadherin, cultured human epithelial breast cancer cells (MCF7; ATCC, Teddington, UK) were used as a positive control. Primary antibodies were diluted in 3% BSA blocking buffer or 3% BSA supplemented with 0.1% Triton (Sigma-Aldrich), as indicated. Cells were exposed to secondary antibodies conjugated to Alexa488 or Alexa568 (1:400; Thermo Fisher Scientific) for 30 min and mounted in VectaShield media containing DAPI (Vector Laboratories, Cambridgeshire, UK). Fluorescence was visualised using a BX51 upright microscope (Olympus) and captured using a Coolsnap ES2 camera (Photometrics). To quantify fluorescence, at least four fields of view per well were analysed and percentage area of staining was calculated with Fiji software. Because of the punctate appearance of HBME1 immunostaining in cultured MCs, positive pixels (raw integrated density) of HBME1 immunostaining was factored for the number of DAPI positive nuclei in each field of view. For analysis of Wt1 immunostaining cells, the percentage of positive nuclei was determined in Image J. For rat omentum and pancreas immunohistochemistry, 15 µm frozen sections were fixed in 4% PFA and immunostained with primary antibodies against HBME1, cytokeratin (C1801, Sigma) or E-cadherin for 48 h at 4˚C and processed for immunostaining as for cultured cells. Tissue sections were imaged by confocal microscopy (Leica TCS SP5 AOBS).

Cell migration assay

A cell culture scratch assay was used [52]. MC monolayers were cultured in media containing 5% FCS overnight before a scratch was created across the well's centre using a 200µl pipette tip. Live cell imaging was performed in a humidified chamber at 37°C and 5% CO_2. Images were obtained every 20 min over 18 h for at least three fields of view per well with at least three wells per condition using an AS MDW live

cell imaging system (Leica) and imaging software Micromanager MM Studio 1.4.20 at x10 magnification.

ELISA

Concentrations of rat BMP4 (CUSABIO, Hubei province, China) and rat IGFBP4 (US Biological, Salem, USA) in culture supernatants were assessed by ELISA according to manufacturers' protocol. Briefly, 100 µl of supernatant was tested in duplicate and optical density values were used to interpolate values from each standard curve. . The lower limit of detection for the BMP4 ELISA was 1.95 pg/ml and for the IGFBP4 ELISA was 156 pg/ml.

TGFβ1-induced peritoneal fibrosis and peritoneal MC lineage tracing in mice

Male C57/BL6J mice aged 8 weeks (Charles River, Harlow, UK) were maintained in SPF conditions with food and water available *ad libitum*. Following acclimatisation, mice received a single intraperitoneal injection of 1.5×10^8 pfu of a first-generation adenovirus expressing the active form of TGFβ1 (AdTGFβ1; kind gift of P. Margetts, McMaster University, Hamilton, Canada) in 100 µl of PBS (n = 5) as previously described [16]. Control mice received 1.5×10^8 pfu of a control adenovirus (AdDL) that lacked transgene expression (n = 5). After 7 days, the entire anterior abdominal wall was resected and the upper portion of tissue was PFA fixed, processed and 7 µm sections collected. Sections were stained with Masson's trichrome or immunostained with primary antibody for pan-cytokeratin (C1801, Sigma). Next, we combined physical injury to the peritoneum by surgical abrasion of adjacent serosa followed by close apposition, as we previously described [17] with a mesothelial lineage tracing strategy, similar to that described by Lua et al. but using *LacZ* rather

than *GFP*, with induced peritoneal injury [18]. Compound mutant mice *Wt1*$^{tm2(cre/ERT2)Wtp/+}$;*B6.129S4-Gt(ROSA)26Sor*$^{tm1Sor/}$ [66, 67], aged 6-8 weeks were administered tamoxifen (Sigma) dissolved in corn oil (10 mg/ml; Sigma) at 1 mg/10 g body weight by oral gavage on 5 consecutive days, followed by 2 weeks washout according to published protocols [67]. Peritoneal adhesion formation was induced by local physical injury under surgery as we previously described [68]. At surgery and at day 1, 3 and 5 thereafter, mouse BMP4 (recombinant carrier-free, BioLegend) reconstituted in 10 mM citric acid was injected intraperitoneally at 300 ng/g body weight using medical-grade saline (50 ng/µl, 0.1% BSA; n=3), while control animals received vehicle saline alone (containing 0.1% BSA and citric acid; n=3). One week after BMP4 or vehicle control administration, caecum-peritoneal wall adhesions and surrounding tissue was collected. Tissue was fixed in 2% PFA/ 0.2% glutaraldehyde, followed by whole mount XGal staining according to published protocols [67]. Images were captured using a Leica DFC420C camera attached to a Leica MZ16F dissection microscope. Regions containing XGal-positive cells in the adhesion zone were dissected and processed into Eosin-stained paraffin sections. Images were captured using a Leitz DM RB microscope with a Leica DFC 450C camera.

Supplementary figure

Supplementary Figure S1. E-cadherin immunostaining of rat omental mesothelial cells. A. Serial rat omental sections were immunostained for HBME1 and Pan cytokeratin to identify the mesothelium and E-cadherin. Note the absence of E-cadherin immunostaining of the omental mesothelium. Sections of nearby rat pancreas used as a positive control were devoid of HBME1 but showed both cytokeratin and intense junctional E-cadherin immunostaining. **B.** Confluent monolayers of cultured sorted rat mesothelial cells showed little positive immunostaining for E-cadherin (Arrow indicates possible weak junctional staining). In contrast, cultured human epithelial breast cancer cells, MCF7, displayed prominent junctional E-cadherin staining. No primary acted as a negative control for tissue sections and cell cultures and nuclei were stained with DAPI. Scale bars are 100μm. **C.** Unsorted and Mojo-sorted MCs displayed comparable CT values for E-cadherin.

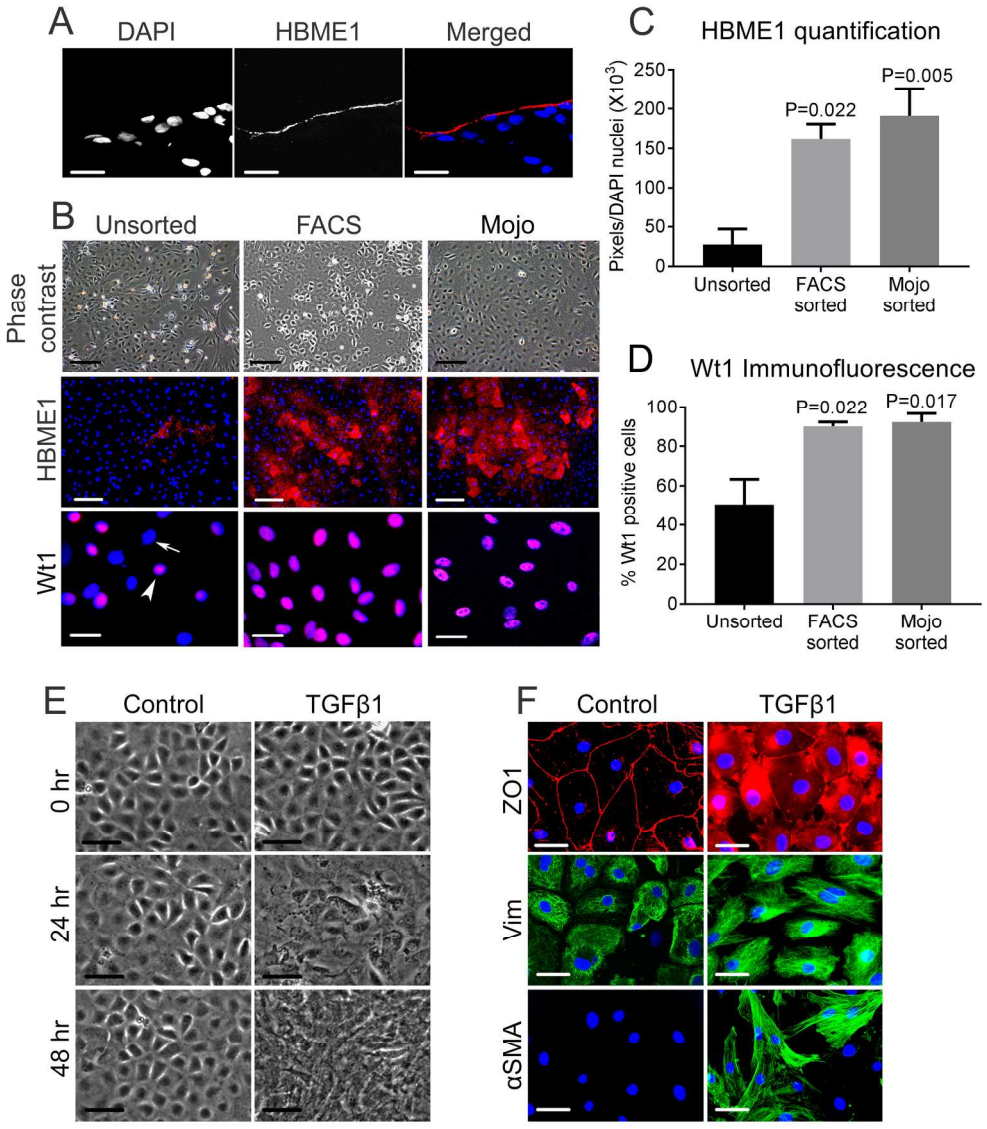

Figure 1. Mesothelial cell enrichment using HBME1 as a surface marker. A. Fluorescence microscopy of rat omentum, showing all nuclei stained with DAPI, the mesothelial cell apical surface immunostained for HBME1, followed by merged overlay image. Scale bars are 50 μm. B. Phase contrast and immunofluorescence images of primary cultures of unsorted, HBME1-FACS sorted and HBME1-magnetic bead (Mojo) sorted cells; note the prominent cobblestone phenotype of the sorted cells. Scale bars are 200 μm. Relative to unsorted cells, both FACS and Mojo sorted cells give an impression of marked enrichment for HBME1. Note the presence of both Wt1+ (Arrowhead) and Wt1- (Arrow) nuclei in the unsorted population stained with DAPI. Scale bars are 50 μm C. Relative to unsorted cells, HBME1 enrichment was confirmed by measuring the pixels of positive immunostaining normalised to DAPI nuclei in FACS sorted (P=0.022) and Mojo sorted cells (P=0.005; n=6; mean±SEM). D. The percentage of Wt1+ nuclei was significantly increased following either FACS (P=0.02) or Mojo sorting (P=0.017; n=3; mean±SEM). E. Cells were maintained for 48 h in either basal media alone, or media supplemented with 1 ng/ml TGFβ1. Note the disruption of the cobblestone phenotype under TGFβ1 treatment, with cells becoming elongated. Scale bars are 50 μm. F. Fluorescence microscopy of cells at 48 h demonstrating that exposure to TGFβ1 was associated with disruption of reticular cell-cell junctional ZO1 pattern with more prominent cytoplasmic

immunostaining for vimentin and αSMA. Nuclei stained with DAPI. Scale bars are 50 μm.

195x226mm (300 x 300 DPI)

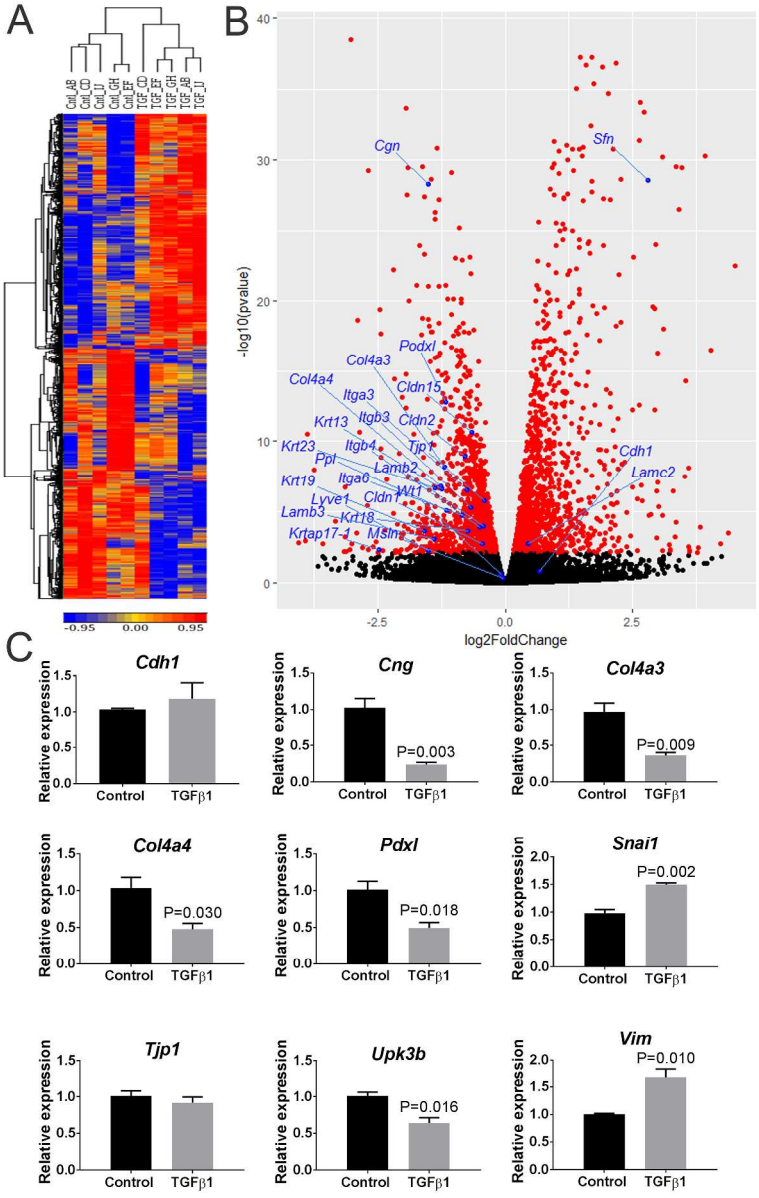

Figure 2. Transcriptome analyses of HBME1-sorted rat mesothelial cells. A. Unsupervised hierarchical clustering by transcript expression. Rows are expression levels denoted as the z-score, displayed in a high-low (red-blue) colour scale, numeric scale indicates z-transformation. Note that levels of numerous transcripts are increased or decreased after 48 h of exposure to 1 ng/ml TGFβ1. 'Cntrl' are the five vehicle-only exposed samples. 'TGF' are the five parallel cultures exposed to TGFβ1. B. Selected RNA-seq data displayed as a volcano plot with the image annotated for 'epithelial signature' transcripts. C. QPCR for *Cdh1*, *Col4a3*, *Col4a4*, *Cng*, *Pdxl*, *Snai1*, *Tjp1*, *Upk3b*, and *Vim* (n=3; mean±SEM).

295x435mm (300 x 300 DPI)

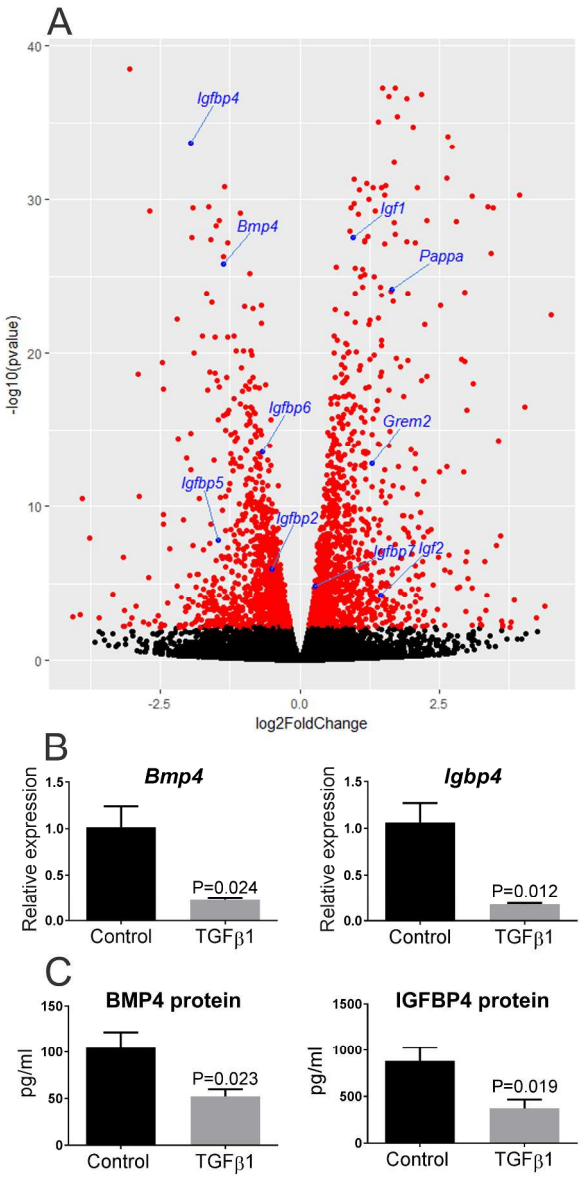

Figure 3. MMT is associated with dysregulation of BMP4 and IGF pathways. A. Volcano plot annotated with transcripts encoding molecules implicated in BMP and IGF signalling. B. Confirmation of decreased levels of *Bmp4* (P=0.024, n=3; mean±SEM), and *Igfbp4* (P=0.012, n=3; mean±SEM) as assessed by QPCR. C. As determined by ELISA, concentrations of BMP4 (P=0.023, n=5; mean±SEM) and IGFBP4 (P=0.019, n=5; mean±SEM) were decreased in media conditioned by cells exposed to 1 ng/ml TGFβ1.

192x369mm (300 x 300 DPI)

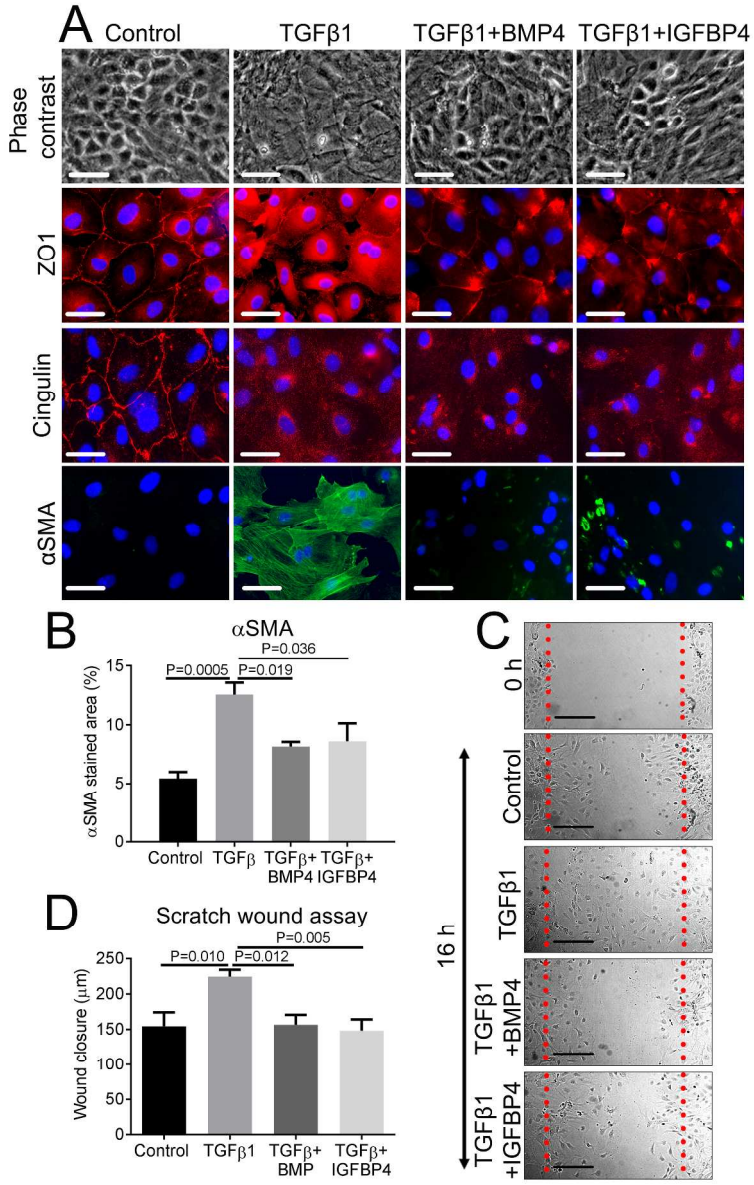

Figure 4. Application of BMP4 or IGFBP4 to TGFβ1-exposed rat mesothelial cells. A. Cells were maintained for 48 h in either basal media alone (Control), media supplemented with 1 ng/ml TGFβ1, or the latter supplemented with either 50 ng/ml of BMP4 (TGFβ1+BMP4) or 50 ng/ml IGFBP4 (TGFβ1+IGFBP4). Cells were imaged by phase contrast (top row) or, as shown in subsequent rows, by immunofluorescence for ZO1, cingulin and αSMA with all nuclei counterstained with DAPI (blue). Note that exposure to either BMP4 or IGFBP4: partially preserved the cobblestone pattern of the monolayer; ameliorated cytoplasmic localisation of ZO1; and reduced αSMA. In contrast, neither factor rescued the TGFβ1-induced disruption of cingulin. Scale bars are 50 μm. B. Quantification of αSMA by immunofluorescence, showing a significantly (P=0.0005, n=5; mean±SEM) increased immunostaining in TGFβ1-treated versus control cells. There was a significant reduction of αSMA expression in cells co-treated with TGFβ1+BMP4 (P=0.019) or TGFβ1+IGFBP4 (P=0.036). C. Phase contrast images showing mesothelial cell migration into a wound over 16 hours under different conditions. Scale bars are 200 μm. D. Quantification of mesothelial cell migration under different conditions (n=6; mean±SEM). Note that TGFβ1 exposure was associated with more extensive migration versus control

(P=0.010 n=6), and that this effect was abrogated when either BMP4 (P=0.012) or IGFBP4 (P=0.005) was added with TGFβ1.

250x390mm (300 x 300 DPI)

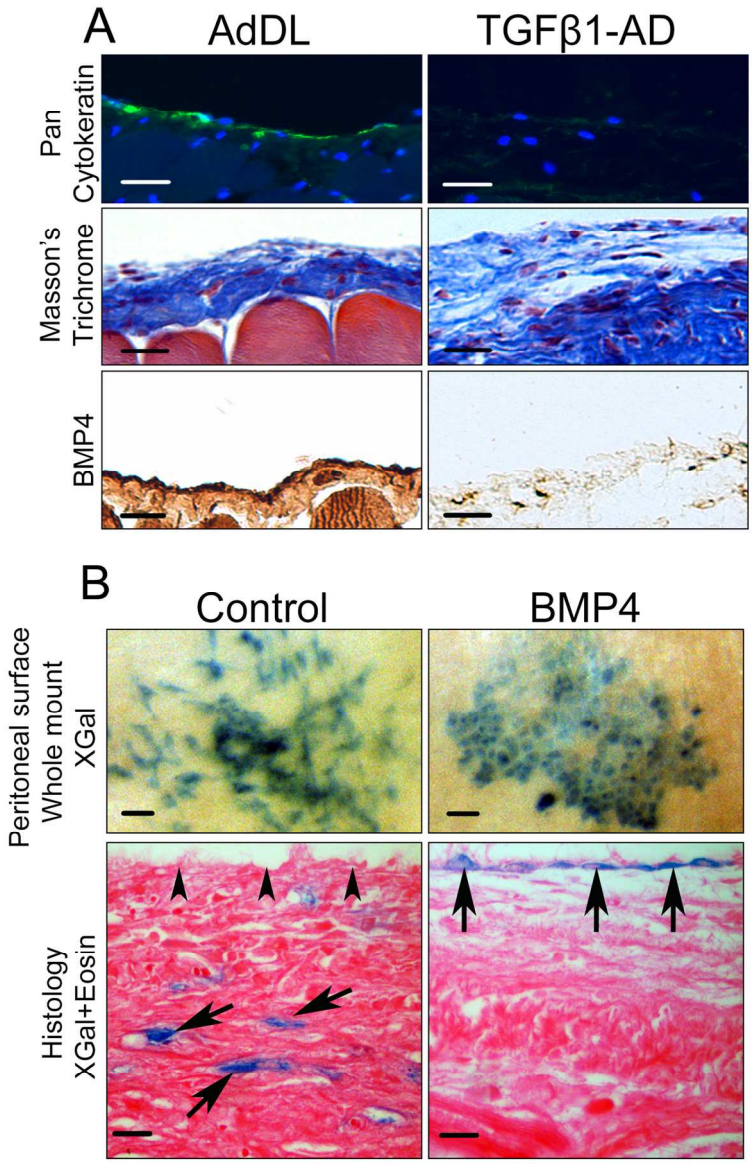

Figure 5. BMP4 in murine models of peritoneal fibrosis. A. Immunostaining for cytokeratin in the peritoneum of mice showed diminished mesothelial-specific expression in response to TGFβ1 adenovirus (AD) compared with control (AdDL) showing nuclei stained with DAPI. In response to TGFβ1 overexpression, the peritoneum was extensively thickened, as shown by Massons trichrome, with near complete loss of surface BMP4 immunostaining. Scale bars are 100 μm. B. Following surgical injury, the peritoneum of Wt1-lineage tracing mice was stained with XGal. Cells expressing the LacZ reporter gene appear blue and represent the fates of subsets of mesothelial cells and/or their progeny. The top two frames show whole mounts, looking down on the peritoneal surface. Injured mice that received vehicle alone (left frame) had elongated and spindle-shaped labelled cells whereas cobblestone-like cell clusters were seen in similarly-injured mice that had received BMP4 (right frame). Scale bars are 100μm. The lower two frames show histology of peritoneum, with eosin (pink) counterstaining: the peritoneal surface is at the top. Injured mice receiving vehicle alone (left frame) showed labelled cells (arrows) below the surface (arrowheads) of the peritoneum. In injured mice that had received BMP4 (right frame), labelled cells (arrows) were noted on the surface of the

peritoneum. Scale bars are 20μm. Representative images from n=3 in each group.

122x172mm (300 x 300 DPI)

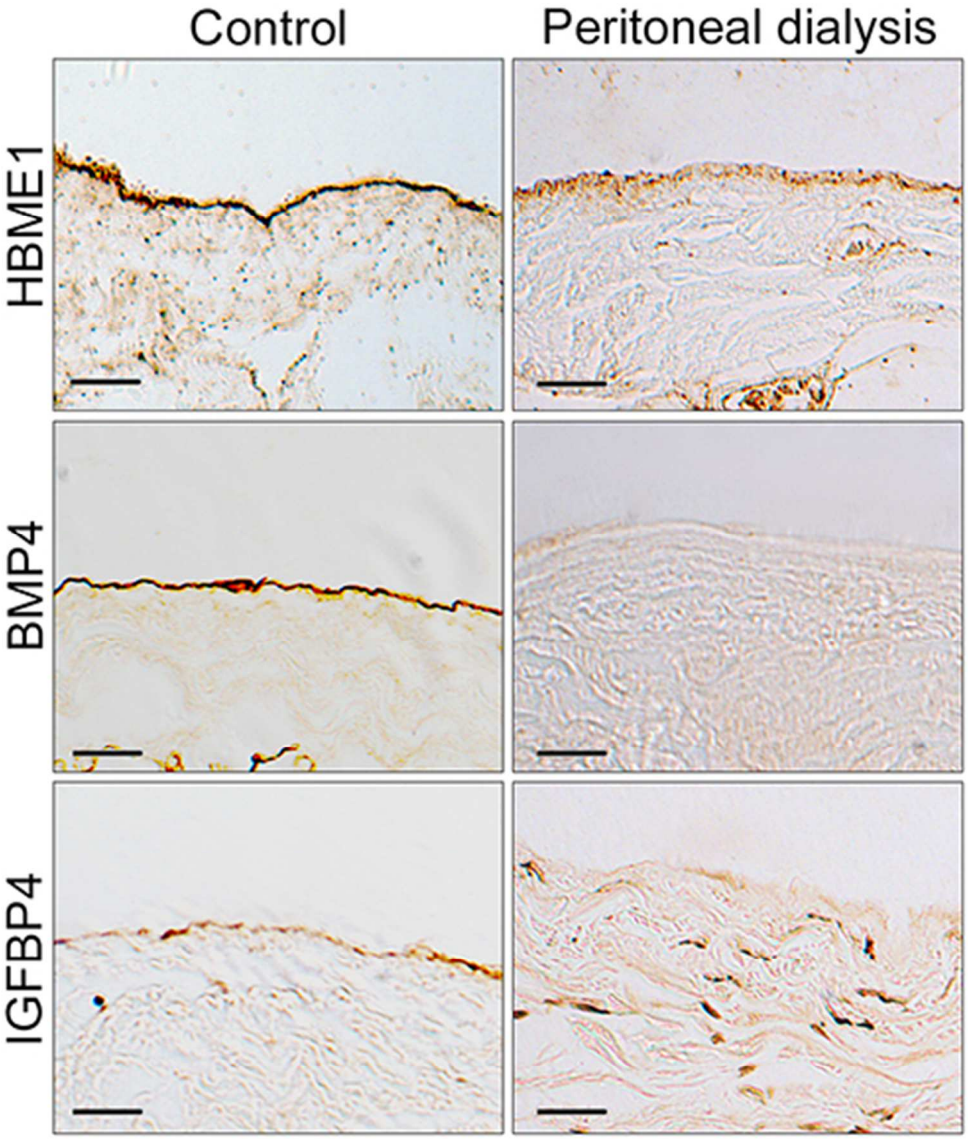

Figure 6. Human fibrotic tissue displays altered patterns of BMP4 and IGFBP4. Human control peritoneum or thickened peritoneum samples from peritoneal dialysis patients were immunostained for HBME1 to identify mesothelium. Control peritoneum displayed prominent mesothelial IGFBP4 and BMP4 immunostaining which was attenuated in peritoneal dialysis samples. In the peritoneal dialysis samples, scattered IGFBP4+ cells were noted below the peritoneal surface. Scale bar is 100 μm.

43x50mm (300 x 300 DPI)

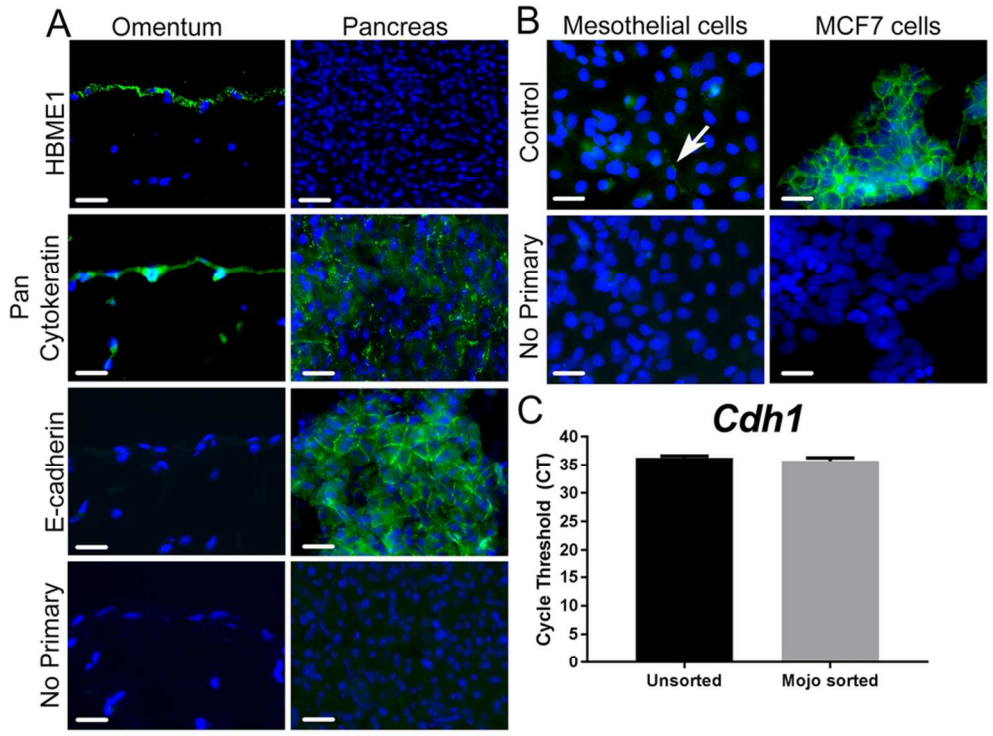

Supplementary Figure S1. E-cadherin immunostaining of rat omental mesothelial cells. A. Serial rat omental sections were immunostained for HBME1 and Pan cytokeratin to identify the mesothelium and E-cadherin. Note the absence of E-cadherin immunostaining of the omental mesothelium. Sections of nearby rat pancreas used as a positive control were devoid of HBME1 but showed both cytokeratin and intense junctional E-cadherin immunostaining. B. Confluent monolayers of cultured sorted rat mesothelial cells showed little positive immunostaining for E-cadherin (Arrow indicates possible weak junctional staining). In contrast, cultured human epithelial breast cancer cells, MCF7, displayed prominent junctional E-cadherin staining. No primary acted as a negative control for tissue sections and cell cultures and nuclei were stained with DAPI. Scale bars are 100μm. C. Unsorted and Mojo-sorted MCs displayed comparable CT values for E-cadherin.

86x66mm (300 x 300 DPI)